Ocean Engineering 266 (2022) 112798

Contents lists available at ScienceDirect

Ocean Engineering

journal homepage: www.elsevier.com/locate/oceaneng

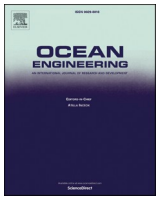

Decarbonizing bulk shipping combining ship design and alternative power

Elizabeth Lindstad [a,*], Dražen Polić [b], Agathe Rialland [a], Inge Sandaas [a], Tor Stokke [c]

[a] SINTEF Ocean, Marine Technology Centre, Trondheim, Norway
[b] Norwegian University of Science and Technology, Trondheim, Norway
[c] Stokke Marine, Tveit, Norway

ARTICLE INFO

Keywords:
Maritime transport
Bulk shipping
GHG
Ship design
Wind assisted propulsion
Alternative fuels

ABSTRACT

The Sixth Assessment Report by the Intergovernmental Panel on Climate Change (IPCC) stresses the urgency to rapidly reduce global Greenhouse Gas (GHG) emissions to contain global warming. The main focus in the design of bulk vessels for several decades has been maximizing cargo-carrying capacity at the lowest build cost. Reduction in energy consumption and emissions, if achieved at all, was heavily limited by the main design focus. This paper decarbonizes bulk shipping by combining ship design and alternative power. The results indicate: First, building more slender bulk vessels that are powered with wind-assisted propulsion reduces fuel consumption and GHG emissions by around 25% at an abatement cost of less than Zero, i.e., free of charge; Second, when combining slender hull and wind-assisted propulsion with Zero-carbon fuels, a 100% GHG reduction comes at an abatement cost of 328 USD per ton of CO_2, which is still significantly less than the 459 USD per ton of CO_2 with Zero-carbon fuels only.

1. Introduction

Maritime transport has dominated and supported trades between regions and continents for centuries. The increased efficiency of sea transport and improvements in communication, market liberalisation, and standardisation have enabled globalization (Kumar and Hoffman, 2002). Today sea transport accounts for 80% of the global trade measured in ton-miles (UNCTAD, 2021) and 3% of GHG emissions (Lindstad et al., 2021). The IPCC sixth Assessment Report (2021) stresses the urgent need for rapidly reducing GHG emissions to mitigate global warming. The European Green Deal follows IPCC (2021) by calling for the EU to become climate-neutral by 2050 and reduce GHG emissions from transport by 90%, compared with 1990 levels. The terms climate-neutral or net-zero do not imply that there will be zero anthropogenic GHG emissions but that all remaining anthropogenic GHG emissions will have to be offset with direct carbon removal from the atmosphere.

The transport sector accounts for nearly 30% of our final Global energy use, i.e., 118 out of 400 Exajoules (Shell, 2021), when measured Tank-to-Wheel for cars and rail, Tank-to-Propeller for aviation, and Tank-to-Wake for ships (for which we use the common acronym TTW). If we include the energy use for producing the fuels, i.e., the Well-to-Tank part, the transport sector's share of total energy consumption is less than 30%. Simply because fuels have lower Well-to-Tank conversion losses than electricity which mainly is produced from coal and gas. A rough estimate will hence be that the transport sector accounts for around 25% of Global Primary energy consumption measured Well-to-Wake (WTW), i.e., 150 out of 600 Exajoules (Shell, 2021). Compared to other transport modes, maritime freight transport is energy efficient, consuming 20% of the energy spent on freight transport (WTW) while performing 80% of the total freight work. In comparison, the remaining 20% of the freight work performed by road, rail, and air consumes 80% of the energy used on freight transport. Despite being 16 times more energy-efficient than the other transport modes on average, there is no doubt that maritime transport also needs to deliver significant energy efficiency and emission reductions. Bouman et al. (2017) propose several improvements to reduce maritime transports energy consumption and GHG: technical improvements to ship systems (including changes in the design), operational changes, switch to greener fuel, or some combination of the mention.

Fuels with zero GHG footprints are made from renewable resources (hydro, wind, or solar), and they come with clear distinction in maritime transport. E-ammonia and E-Hydrogen do not share many properties with today's fuels, e.g., conventional diesel (MGO) and liquefied natural gas (LNG). Therefore, their potential implementation requires new vessels and bunkering infrastructure. In contrast E-Diesel, E-LNG, and E-Methanol made from renewable electricity and direct capture of CO_2

* Corresponding author.
E-mail address: Lindstad@sintef.no (E. Lindstad).

https://doi.org/10.1016/j.oceaneng.2022.112798
Received 28 June 2022; Received in revised form 19 September 2022; Accepted 2 October 2022
Available online 14 October 2022
0029-8018/© 2022 The Authors. Published by Elsevier Ltd. This is an open access article under the CC BY license (http://creativecommons.org/licenses/by/4.0/).

Nomenclature

Abbreviation

AWA	Apparent wind angle
AWS	Apparent wind speed
CAPEX	Capital expenditure
DWT	Deadweight tonnage
EEOI	Energy Efficiency Operational Indicator
GHG	Greenhouse Gas
HFO	Heavy fuel oil
IPCC	Intergovernmental Panel on Climate Change
LCA	Life cycle assessment
LDT	Light displacement
LNG	Liquefied natural gas
LOA	Length overall
MGO	Marine gas oil
nm	Nautical mile
OPEX	Operating expenses
RPM	Revolutions per minute
SFOC	Specific fuel oil consumption
TC	Time charter
TCE	Daily time charter equivalent cost
TOE	Tons of oil equivalent
TTW	Tank-to-Wake
TWA	True wind angle
TWS	True wind speed
VLSFO	Very Low Sulphur Fuel Oil
WASP	Wind-assisted ship propulsion
WTT	Well-to-Tank
WTW	Well-to-Wake

Symbol

B	Ship beam, m
C	Cost per nautical mile sailed, USD/nm
c_w, k_w	Weibull distribution parameter
D	Distance of the voyage, nm
F	Fuel consumption, metric ton (all tons are metric)
Hs	Significant wave height, m
K_{ep}	CO_2 emission factor for the fuel, CO_2/ton
K_f	Engine consumption at the optimal load, ton/kWh
L	Ship length, m
L_{BWL}	Length of the bow on the water line, m
M	Mass, ton
P	Power, W
R	Resistance, N
T	Ship draught, m
T_{wind}	Thrust produced by wind, N
TCE	TCE, USD
TWS	TWS, m/s
v	Ship speed, nm/h (knot)
v_b	Hull boundary speed, m/s
∇	Displacement, m^3
ε	CO_2 emissions, g/(nm•ton)
η	Propulsion efficiency

from airshare main properties with today's fuels. Their implementation requires hence no modifications for vessels switching from conventional diesel to E-Diesel or from LNG to E-LNG. Furthermore, if the engine and fuel system onboard the vessels are built with the conversion in mind, switching from conventional bunker oil or MGO to E− or Bio-methanol is simple, and there is no need for new vessels (Svanberg et al., 2018; Lindstad et al., 2021).

The term Low Carbon fuel is frequently used for both Biofuels and fossil fuels having lower GHG emissions per energy unit than the conventional diesel (MGO) or bunker oil (HFO, VLSFO). Compared to fossil fuels, the variation in biofuels' well-to-tank emissions is of much larger scale due to their different sources of origin and the indirect effects on land use. For example, while Biogas might be close to zero in GHG emissions, Biodiesel made from Palm oil can potentially more than double the emissions compared to the fossil fuels (SSI, 2019). LNG and LPG made from fossil sources are often included as low GHG fuels, since they have 15–20% lower GHG emissions than conventional fuels measured Well-to-Wake (Lindstad et al., 2020).

The power used to move the ship is a function of the ship's speed to the power of three to four (Kristensen, 2010), implying that the fuel consumption per freight work grows significantly with the ship's speed. Therefore, many authors (e.g., Corbett et al., 2009; Psaraftis and Kontovas, 2010; Lindstad et al., 2011) argue for speed optimization and reduction. However, most of the potential for reduction through speed optimization has already been achieved through lower operational speeds (slow steaming) coming from overcapacity in the shipping market since the financial crisis in 2008 (Smith et al., 2015; Fairplay, 2018). Several authors (Bausch et al., 1998; Fagerholt, 2001; Norstad et al., 2010) have also incorporated speed optimization into the routing decisions and showed that the speed optimization could result in significant fuel savings. However, the shown fuel savings cannot be utilized as long as the speed optimization omits port planning (Alvarez et al., 2010); where berthing policies used at ports often admit vessels on a first-come, first-served basis. Finally, any change in speed will also affect the number and size of vessels within a given fleet, in order to maintain a similar service level and delivery capacity (Cho and Perakis, 1996; Fagerholt and Lindstad, 2000; Christiansen et al., 2007; Fagerholt et al., 2009).

Traditionally, research on hull shapes and propeller design has focused on optimising for still-water conditions with design cargo loads and design speeds beyond the boundary speed. For any given hull form, the boundary speed[1] can be defined as the speed range where the total still (calm) water resistance coefficient goes from practically constant to rising rapidly, thus making further rises in speed prohibitively expensive (Silverleaf and Dawson, 1966). In practice, the combination of a calm sea with design loads and speed is the exception rather than the rule (Faltinsen et al., 1980). Hirota et al. (2005) show how hull form can be optimised to minimise fuel consumption in waves rather than in calm water. Similar results have been found by Kristensen (2010); Stott and Wright (2011); Lindstad et al. (2013) who have investigated how to make hull forms more energy efficient under realistic sea conditions by modifying the main ratios between beam, draught, and length to reduce block coefficients[2] while keeping the cargo-carrying capacity unchanged. By reducing the block coefficient, the hull form becomes slender, the boundary speed increases, and higher operational speeds are enabled. Consequently, the slender hull has lower fuel consumption for the same ship speed compared to the more full-bodied design counterpart.

Wind-assisted propulsion has been reborn in recent years in the research community (Rehmatulla et al., 2017; Lu and Ringsberg, 2020; Chou et al., 2021) as an answer to the public demand for emission reduction and decarbonization of the maritime sector (Council of the

[1] $V_b = (1.7 - 1.4 * C_b) * \sqrt{\frac{L}{0.304}}$ Here, C_b is the block coefficient and $L$is the length of a ship in the waterline from the forward stern or forward perpendicular, to the sternpost or aft perpendicular. The constant: 0.304 converts the ship length in meter to feet. The Boundary speed is given in knots.

[2] Block coefficient: $C_B = \frac{\nabla}{L \bullet B \bullet T}$ where ∇ is the displaced volume, L is length, B is beam and T is draught.

European Union, 2015). The potential of wind-assisted propulsion depends on how efficiently the ship counterbalances the side force generated from sails (a generally unwanted effect caused by the aerodynamic drag). Current ship hull and propulsion solutions are not constructed on the principle where additional thrust and side forces are generated from a sail (Rojon and Dieperink, 2014), and retrofitting large sails may cause more harm than good. For example, if the hull has a limited capacity to counteract the side force, the high rudder angle will correct most of the force; Kramer and Steen (2022) showed that the rudder could cause significant wind-induced hydrodynamic resistance at high angles. Therefore, two to three times greater utilization of the wind power is expected with newbuild ships (Kramer et al., 2016; Rehmatulla et al., 2017; Chou et al., 2021). Besides the design of the hull and appendages to take side force with minimum added resistance, the speed of a wind-assisted ship is important. Hydrodynamic forces on the hull and appendages are a function of the ship's speed to the power of two. Changes in the design and potentially higher operational speeds of the ship align with Lindstad et al. (2022). They found that by expanding length to enable more slender hull forms and keeping cargo capacity unchanged, fuel consumption and emissions can be reduced by up to 40% on an operational basis (EEOI) and 30% when shipbuilding is included (LCA).

Based on the above, we can conclude that there is a rich literature on improving maritime transport and reducing cost, fuel, and emissions per freight unit transported. However, very few studies have investigated combining multiple measures for ocean-going vessels (Bouman et al., 2017; Balcombe et al., 2019), such as ship design and alternative power, including both fuels and wind. The motivation for our study is: First, to see the benefits of a slender hull combined with wind-assisted propulsion (WASP), and second, to compare 100% decarbonized ship with and without a slender hull and WASP. The benefits are evaluated based on the potential energy and emission reductions and cost implications. The paper proceeds as follows: The employed model is described in section 2; the case study ship and systems are presented in section 3; the obtained results and analysis are presented in section 4, and the conclusion in section 5.

2. Model description

The main objective of the model is to calculate power, fuel consumption, and costs for the alternative designs when employed with more realistic sea trades. The first Eq. (1) gives the required power from the ship engine(s) to push the ship (Lewis, 1988; Lloyd, 1998; Lindstad et al., 2013, 2022). It includes power components needed to overcome still-water, waves, and air resistance, abbreviated as P_s, P_w, P_a, respectively. In addition, the propulsion efficiency η, auxiliary power P_{aux}, and power generated by the WASP device P_{wind} are included in Eq. (1).

$$P_i = \frac{P_s + P_w + P_a}{\eta} + P_{aux} - P_{wind} \quad [1]$$

The software package NAPA has been applied to create alternative designs based on a reference vessel and its associated towing tank results, drawings, weights, and other technical data. Holtrop (1984) is used for the required calm-water power, and the added resistance in waves is based on the STA-wave1 method given by Eq. (2) (van den Boom and Hasselaar, 2014; ITTC, 2014).

$$R_{aw} = \frac{1}{16}(\rho \bullet g \bullet H_s^2 \bullet B)\sqrt{\frac{B}{L_{BWL}}} \quad [2]$$

ρ is the density of seawater, g is the gravity, B is the vessel beam, L_{BWL} is the length of the bow (from the tip to 95% of the maximum beam on the waterline), H_s is the significant wave height.

A common way to describe the annual wind speed distribution is by using the Weibull distribution. The curve represents a fit of the probability density per true wind speed (TWS) at a given location. It is based on exponential regression and described by two parameters: a scale parameter c_w, related to the annual mean TWS, and a shape parameter k_w describing the variability about the mean. Eq. (3) represents the Weibull probability density function:

$$f(TWS) = \frac{k_w}{c_w}\left(\frac{TWS}{c_w}\right)^{k_w-1} e^{-\left(\frac{TWS}{c_w}\right)^{k_w}} \quad [3]$$

Based on sixty thousand observations made by ships in 1983, Pavia and O'Brien (1986) derived c_w and k_w parameters for Atlantic, West Pacific, East Pacific, and Indian oceans for every month and 5° of latitude. Typical values used today by the offshore wind industry (van der Tempel, 2006) and used in this paper for c_w and k_w are 11.3 and 2.2, respectively. Fig. 1 shows the applied true wind probability distribution. Such c_w and k_w values give an average annual speed of 10 m/s and they are valid for the north section of each ocean, including the Indian Ocean, for most of the year (Pavia and O'Brien, 1986). The south section of each ocean, interpolated from limited data due to the few shipping routes, has an average annual wind speed of 8 m/s. Due to the lack of information, we assumed that all true wind angles are equally possible. A true wind speed range presented in Fig. 1, according to the Pierson-Moskowitz spectrum, can generate a broad significant wave height spectrum (also given in Fig. 1). However, using the wind-probability to weight wave heights, the average significant wave height calculated from spectrum is 2.75m (see dashed blue line in Fig. 1). The average significant wave is used in section analysis as one of the arguments for selection of representative wave heights.

The thrust and side force generated by a Flettner rotor on board a ship is computed based on the lift and drag coefficients given in Tillig and Ringsberg (2020). The coefficients are validated with full- and model-scale data for a particular Flettner rotor design (height over diameter ratio of six and an endplate disc diameter twice the rotor's diameter) and expressed as a function of the spin ratio. The spin ratio compares the local apparent wind speed (AWS) with the tangential Flettner rotor speed. The local AWS is a vector sum of the headwind speed (negative ship speed) and TWS. Due to the wind shear, the AWS varies over heights, as does the angle of attack. The friction between wind and Earth's surface causes the TWS to be zero at the water surface. Wind shear is considered by the power-law coefficient $\alpha = 0.15$ given in the wind offshore standard IEC 61400–3:2019 (IEC, 2019). Following a strip-theory approach and a quasi-steady approach, the apparent wind

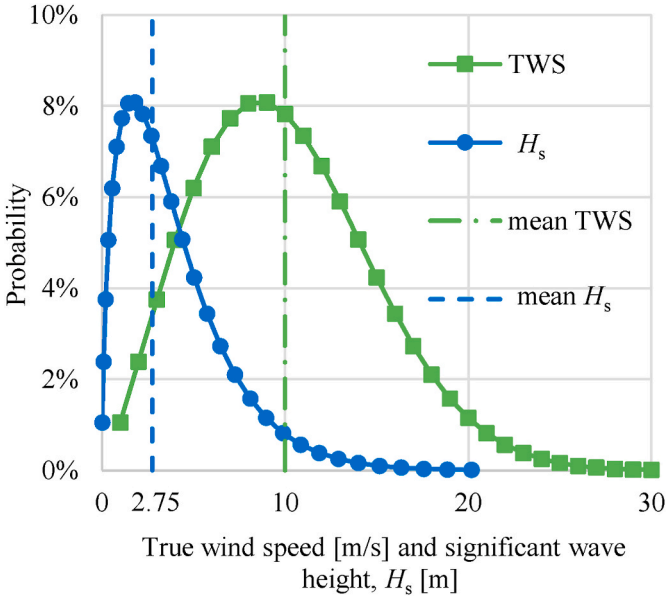

Fig. 1. Wind and wave probability distribution.

speeds and angles (AWA) were evaluated for each strip of the rotor. Using AWS and AWA for each strip, the aerodynamic lift and drag force vector are expressed and transferred to a ship-fixed coordinate system as thrust and side force. The total global load from four Flettner rotors was then found by summation over all strips and the number of rotors. The same approach is used for the required power, and the total power generated by the installed WASP is expressed as:

$$P_{wind} = \left(T_{wind} - R_{add,wind}\right) \bullet 3600/1852 \bullet v_i - P_{req,WASP} \quad [4]$$

T_{wind} is thrust in N produced by WASP, $R_{\text{add,wind}}$ is added wind-induced hydrodynamic resistance caused by WASP, v_{i} is ship speed, and $P_{\text{req,wasp}}$ is WASP required power.

The added wind-induced hydrodynamic resistance is assumed to be proportional to the side force. Three proportionalities were checked: zero, one, and 0.5. Such simplification of the hydrodynamic hull lift and drag ratio disabled the possibility to evaluate ship drift angle and potential gains or losses generated by the change in the wind angle of the attack on the rotor. Note that the presented approach also excludes the de-powering of the rotor when the ship is healing and assumes that the rudder can balance the yaw moment generated by the rotors. The interaction between Flettner rotors and other superstructures was neglected, a valid assumption in apparent beam wind conditions, but which becomes questionable close to headwind and tailwind conditions (Garzon and Figueroa, 2017; Bordogna et al., 2019).

Eq. (5) gives the building cost *Capex*, for the alternative ship designs based on the building cost of the reference vessel.

$$Capexv_{New} = Capexv_{Ref} \bullet \left(1 + \sum_{j=0}^{n} \left(\Delta_j\right)\right) \quad [5]$$

Eq. (6) gives the daily time charter equivalent cost (TCE), for each design.

$$TCE = Capex + Opex \quad [6]$$

TCE expresses the required payback for the new vessel over a depreciation period of 15 years and considers all the operational costs (*Opex*) and the required return on the owner's capital (*Capex*). Over these 15 years, it is expected that Time Charter (*TC*) will go above (good market) and below (poor market) TCE.

Eq. (7) gives the fuel consumption per voyage.

$$\mathrm{F} = \sum_{i=0}^{n} \left(\frac{D_i}{v_i} \bullet \left(\left(K_f \bullet P_i\right) \bullet \left(1 + \left(0.75 - \frac{P_i}{P_{tot}}\right)^2\right)\right)\right) \quad [7]$$

Each voyage is divided into n legs, with a leg distance of D_{i}. The time spent on the leg i of the voyage is set by the first factor (D_i/v_i), while the remaining factors give the fuel consumption in the same leg. K_f is the fuel consumption per produced kWh at the engine's sweet spot, P_{i} is the power required as a function of sea conditions, P_{tot} is the total available propulsion power that includes the power needed for auxiliary and hotel load. The approximation given by $\left(1 + \left(0.75 - \frac{P_i}{P_{tot}}\right)^2\right)$ replicates a typical fuel consumption curve with high fuel consumption per kWh at low power. Such approximation implies nearly flat consumption from 60% to 90% of max available power and a gradual increase up to 100% of max available. The variation in the sea condition is captured by splitting the leg and changing P_{i} and ship speed v_i. Fuel consumption in ports and at anchor is ignored in all cases. Eq. (8) gives the CO_2 emissions per ton nm

$$\varepsilon = \frac{F}{M \bullet D} \bullet K_{ep} \quad [8]$$

K_{ep} is the CO_2 emission factor for the fuel. D is the distance sailed and M is the mas of the cargo transported.

Eq. (9) gives the cost per nautical mile sailed which includes the fuel cost and *TCE*.

$$\mathrm{C} = \frac{1}{D}\left(\sum_{i=0}^{n} \frac{D_i}{v_i}\right) \bullet TCE_v + F \bullet Fuel_{cost} \quad [9]$$

$Fuel_{cost}$ is the cost per ton of fuel equivalent.

3. Data set

This paper focuses on decarbonizing Bulk shipping by combining ship design and alternative power. The global dry bulk fleet is responsible for transporting nearly 50% tons of the global sea transport measured in tons transported and more than 40% of the freight work measured in ton-miles (Bengtsson, 2018). The dry bulk fleet consists of nearly 12 000 vessels (Lloyd's List Intelligence, 2019), and one-quarter of the fleet are Supramax vessels with deadweight (dwt) in the 52 000–67 000 range, where the term Ultramax generally is used for the largest ones, i.e., in the 64 000–67 000 range. Supramax vessels are commonly built with five cargo holds and four slewing cranes. The installed cranes enable servicing ports without cranes and cargo transshipments to or from a barge or smaller vessels at sea. Furthermore, the hatch covers and decks can often carry deck cargo to increase cargo intake or for cargo unsuited for cargo holds. Their typical main dimensions are 200m in length, 13.4m in draught, and beam width up to 32.3m (restrictions of the old Panama Canal locks), with block coefficient is in the 0.86–0.90 range, to maximize cargo-carrying capacity. This has resulted in full bodied (shoebox-shaped) vessels with short bow and aft ship sections and hence rather poor hydrodynamic lines and high resistance even in calm seas. In rough seas, these designs perform even worse compared with vessels with the same cargo-carrying capability designed for good hydrodynamic performances. Historically this has still paid off, because apart from a few price hikes in 2007–2008 and 2012–2014, fuel prices have been generally low so even if consumption has been high the total fuel cost has remained small compared with the fixed costs of a bulk vessel, its crewing and management. Today, however, fuel might account for more than 50% of the total costs, which in combination with stricter energy efficiency requirements, makes design improvement to reduce fuel consumption more attractive and even a necessity for all new bulk vessels. This is in contradiction with traditional bulk vessel designs, where the focus has been on maximizing the cargo-carrying capacity at the lowest possible building cost and not on minimizing the energy consumption.

Previously, Lindstad et al. (2019) have investigated expanding the length of a Supramax with 10–15% to enable more slender hull forms without decreasing the cargo-carrying capacity. Lindstad et al. (2022) also combined the long and slender Supramax with wind-assisted propulsion. Since the Supramax and Ultramax vessels are partly operating in the same trades as the larger Kamsarmax vessels with deadweight in the 80–85 000dwt range, expanding length above 200m will mathematically only exclude a limited number of trading options. Still, going beyond standards is often seen as a commercial disadvantage. In addition, expanding length increases the building cost and hence the fixed cost of the vessel, so even if fuel savings of 25–35% are within reach for these long and slender Supramax vessels with WASP (Lindstad et al., 2022), we need fuel prices at the present peak crude oil levels of around 100USD per barrel if these vessels shall be cost competitive against the full bodied Supramax vessels. Therefore, we found it relevant to flip the coin and investigate cost, fuel, and emission when keeping the 200m length and instead increasing the maximum draught to enable more slender hull forms without reducing the cargo carrying capacity. The main dimensions of the reference 200m Supramax vessels are given in Table 2 first column, for which a detailed hull shape design already existed in the NAPA tool. Increasing the maximum draught from 13.4m to 14.4m in NAPA enabled us to reduce the block coefficient from 0.88 to 0.79 and keep the dwt unchanged at 63 000 tons (62 800 ton with the four Flettner rotors). Local hull features near the vessel ends where manually adjusted into realistic hull shapes as scaling distorts local

shapes near the bow and stern. While length restrictions are absolute bottlenecks that prevent vessels from entering ports or terminals, draught is a soft constraint, implying that by short loading up to the maximum available draught, the vessel can still be employed in the trade. Due to the "economy of scale" effect, there is a continuous process of shifting trades to ports accepting larger vessels, and gradually increasing the allowed maximum draught and lengths in existing ports. Cost-wise, when comparing increasing length and draught, increasing length is costly, while increasing draught in combination with a more slender design keeps building cost nearly unchanged. This implies that the fuel and emissions reductions achieved by the 200m Slender Supramax even with WASP will come at an abatement cost close to zero, i.e., free of charge.

Out of five commercially available wind-assisted ship propulsion (WASP) solutions (Flettner rotors, Kites, Rigid sails, Soft sails, Suction wings), we selected Flettner rotors as the most mature solution. Flettner rotors give the most aerodynamic lift per sail area; hence, they are one of the smallest devices. Flettner rotors can also tilt and enable smooth port and cargo handling operations. The vessel is therefore designed with four tiltable rotors spaced 29.6m between each and positioned at hatch ends on the port side. Fig. 2 shows the average effective net propulsion power generated with these four rotors if the 200m slender Supramax is employed in typical worldwide trades. Fig. 3 shows two illustrations of the 200m Slender Supramax with four Flettner rotors, one seen from the front and the other from the aft.

The selected Flettner rotor dimensions and operational constraints, presented in Table 1, are interpolated based on the existing rotor designs and technical information published by three producers: Norsepower, Eco Flettner, and Anemoi. Base height and maximum rotor speed are interpolated based on the rotor diameter, while weight, installed power, and maximum thrust are interpolated based on the sail area. Note that the rotor aspect ratio (height/diameter) is 12% above Tillig and Ringsberg (2020) theory. In addition, it is assumed that the carrying capacity of rotor bearings and foundation is the same in the longitudinal and perpendicular directions. Therefore, the rotor's maximum allowed side force equals the maximum thrust. The optimal RPM of the rotor is determined by maximizing the effective propulsion power (Eq. (4)).

The range of tested RPM is set by the apparent local wind, rotor spin ratio limits, and rotor maximum RPM. The apparent local wind experienced by the rotor is calculated by varying every half knot of ship speed and every true wind speed and angle; increments are 1 m/s and 5°, respectively. As explained earlier, each 1m tall strip of the rotor will have different apparent wind and, consequently, a different spin ratio, as all strips rotate with the same RPM. The minimum rotor RPM for each combination of the true wind and ship speed is computed by considering the strip with the weakest apparent wind and a spin ratio of one. The maximum RPM is set by the lowest of two conditions; the maximum design RPM or a spin ratio of three combined with the strip with the strongest apparent wind. The limits of one and three for spin ratios are taken from Tillig and Ringsberg (2020). Considering increments of 5 RPMs, the rotor RPM varies from the minimum to the maximum value. To prevent an infinite generation of the side force while maximizing effective power, we disregarded all power results obtained with the thrust force smaller than the side force.

The average net propulsion power, shown in Fig. 2, for every ship speed is evaluated by multiplying the probability and maximum effective power generated by WASP for each wind condition. The probability of each wind condition is derived by dividing TWS probability by the number of simulated angels.

The main observations from Fig. 2 are: First that if we can take up all side forces created by the wind through the hull, rudders, and appendixes without generating any additional drag (resistance), we can get out a net average propulsion power of 700–1200 kW when operated at typical speeds of 9–12.5 knots for these vessels. The highest values, i.e., *coefficient =0 Smart* reflects a combination of routing to avoid head winds and that Flettner Rotors are laid down if strong headwinds cannot be avoided; Second, if the side forces taken up through the hull, rudders and appendixes generate drag equal to the half of side force, we will get a net propulsion power of 400–600 kW on average from the Flettner Rotors. The 400–600 kW are of the same magnitude as what we get when applying the wind calculation tool by Lloyds Register (LR, 2021); Third, if we are inefficient in avoiding the added drag caused by the side force (*coefficient = 1*), the benefits of the Flettner rotors will be around one-quarter of the one predicted by *coefficient = 0*; Fourth, for this study, we assume that the propulsion power from the WASP units will be in line with the *coefficient = 0.5 smart*, because the tiltable rotors will be laid down on routes with strong to headwind conditions and moderate adjustments of routings will be made to utilize the wind.

For Zero carbon fuels we limited ourselves to E-ammonia which, compared to other E-fuels, comes at the lowest fuel cost per energy unit. Table 2 displays technical specifications and building cost for: First a typical Supramax 200m; Second a typical Supramax 200m to be fueled by E-ammonia; Third a slender Supramax 200m with WASP; Fourth a 200m slender Supramax with WASP and powered by E-ammonia. The implications for cargo carrying capacity when the Supramax ship is powered on ammonia is a reduction of 3500 tons (Lagemann et al., 2022) compared to when running on conventional bunker oil (VLSFO). The cost values for the investigated designs, as specified by Table 2, are based on new building and prices quoted in the market. Moreover, the additional newbuilding cost enabling to run on ammonia are based on Lindstad et al. (2021). For the combination of Slender, WASP and ammonia we assume that tank capacity can be reduced by 25–30% due

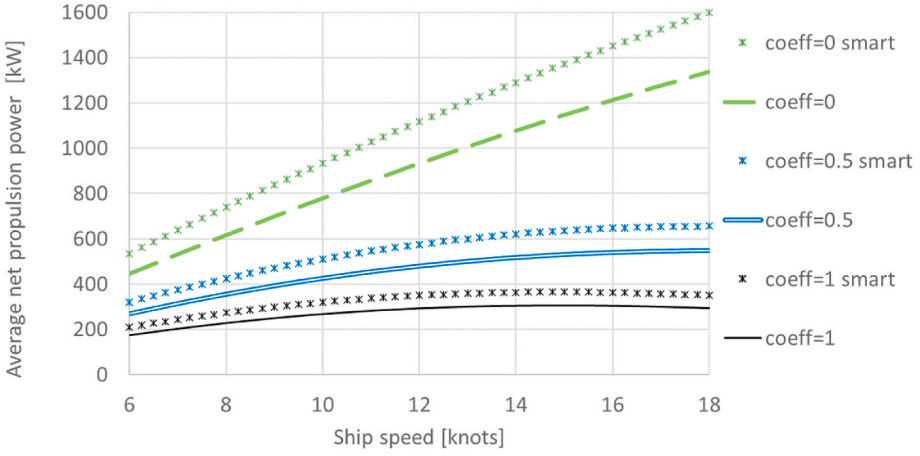

Fig. 2. Average effective propulsion power from 4 Flettner Rotors on a Supramax Dry bulker.

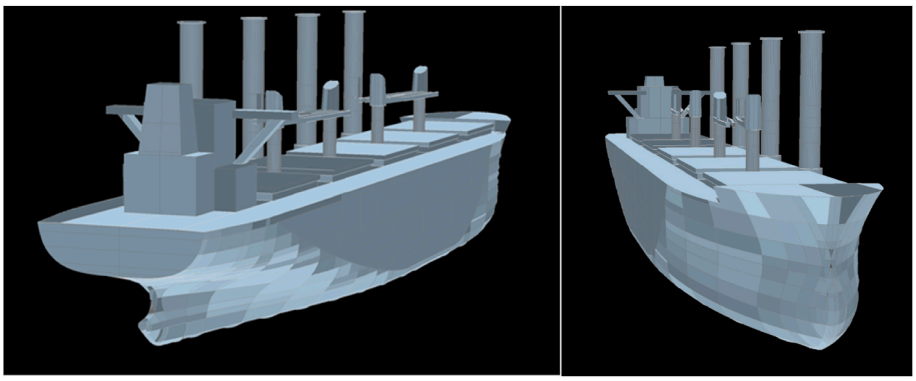

Fig. 3. The 200m Slender Supramax with 4 Flettner rotors.

Table 1
Flettner rotor dimensions and operational constraints.

Height	26	m
Diameter	4	m
Max. rotor speed	225	rpm
Base height	2.5	m
Sail area	327	m^2
Weight	50	t
Installed power	90	kW
Max. thrust	189	kN

Table 2
The Investigated designs.

Vessel		Supramax 200m		200m Slender Supramax & WASP	
Fuel		VLSFO	E-Ammonia	VLSFO	E-Ammonia
LOA (m)		200	200	200	200
Beam (m)		32.3	32.3	32.3	32.3
Displacement (Ton)	11.7 (m)	64 300	64 300	57 900	55 800
	13.4 (m)	73 700	73 700	66 700	66 700
	14.4 (m)			73 700	73 700
Volume capacity (m^3)		79 000	79 000	77 000	77 000
Block – Cb		0.88	0.88	0.79	0.79
Bow length – L_{BWL} (m)	15.5	15.5	38.8	38.8	
Boundary speed (knots)		11.7	11.7	15.1	15.1
LDT (Ton)		10 700	10 900	10 700	10 900
Dwt (Ton)	11.7 (m)	53 600	50 100	47 200	44 900
	13.4 (m)	63 000	59 500	56 900	54 600
	14.4 (m)	N.A	N.A	62 800	60 500
Main Power (kW)		8 500	8 500	8 500	8 500
Newbuild Cost (MUSD)		30	38.5	33.5	40

to its lower fuel consumption. To keep it simple, the reduced cargo carrying capacity when running on ammonia is handled by reducing the deadweight.

The installed propulsion power is kept equal for all ship designs; 8500 kW. The auxiliary power consumption is assumed to be 5% of installed propulsion power, i.e., 425 kW and constant in ports and at sea. The main engine specific fuel oil consumption (SFOC) is 170 g/kWh (engine's sweet spot), which in combination with Eq. (7), gives the engine fuel consumption over a wide load range. Cost per nautical mile sailed includes daily Capex and Opex, fuel consumed at sea while steaming, and annual sailed distance as a function of speed and number of sailing days. Daily Capex and Opex are estimated at 8% and 4% of the annual newbuilt cost, respectively. The full calendar year is used to derive daily costs, while the number of sailing days is assumed to be 237 (65% of a year, a common practice in bulk shipping). The 65% sailing time implies that all additional costs compared to the typical Supramax powered by VLSFO must be earned back at sea, and therefore, the performance is based on sailing cost at sea. We used 500 and 1000 USD per ton of oil equivalent (TOE) for VLSFO to reflect two future scenarios. The lower price reflects 2021 price levels, and the higher, March 2022. For the E-fuels, we use 1750 USD per TOE of E-ammonia (Lindstad et al., 2021) based on renewable electricity prices of 60 USD per MWh, reflecting the average prices needed for new renewable capacity to be profitable. In addition, to match the high prices of conventional fuels seen in March 2022, we also used an E-ammonia price of 2975 USD per TOE (corresponding to a renewable electricity price of 120 USD per MWh). All comparisons are based on a 13.4m draught.

The main observation from Fig. 3 is the much longer bow and aft sections compared to a Typical Supramax reflecting that the block coefficient has been reduced from 0.88 to 0.79, which gives a higher boundary speed and lower fuel consumption both at calm water and in real sea conditions.

4. Analysis

In this section, first, we investigate the potential energy and emission reductions and cost implications when combining slender designs with wind assisted propulsion (WASP); Second, we compare the cost of a 100% decarbonising through zero carbon fuels only, with the cost if zero fuels are combined with slender designs and wind assisted propulsion.

The absolute required power, including auxiliary, for the 200m Slender Supramax and the Supramax 200m as a function of vessel speed under three sea conditions when both are loaded to a draught of 13.4 m is given in the top row of Fig. 4. The middle row shows power savings for the 200m Slender Supramax compared to the Supramax 200m, and the bottom row shows the power savings per dwt capacity. The lower dwt capacity of the 200m Slender Supramax, i.e., 56 900 ton versus 63 000 ton for the Supramax 200m when both are loaded to 13.4m draught, explains why the percentage saving with the Slender Supramax is lower per ton than in the bottom part of the figure, compared to when we just compare on a vessel level. The left column shows the calm water condition, the right column is with 3m significant head waves (6 Beaufort wind scale), and the middle has a 50/50 mix of two conditions. Over a year, vessels experience waves from all directions, where following waves tends to give a small reduction of required power compared to

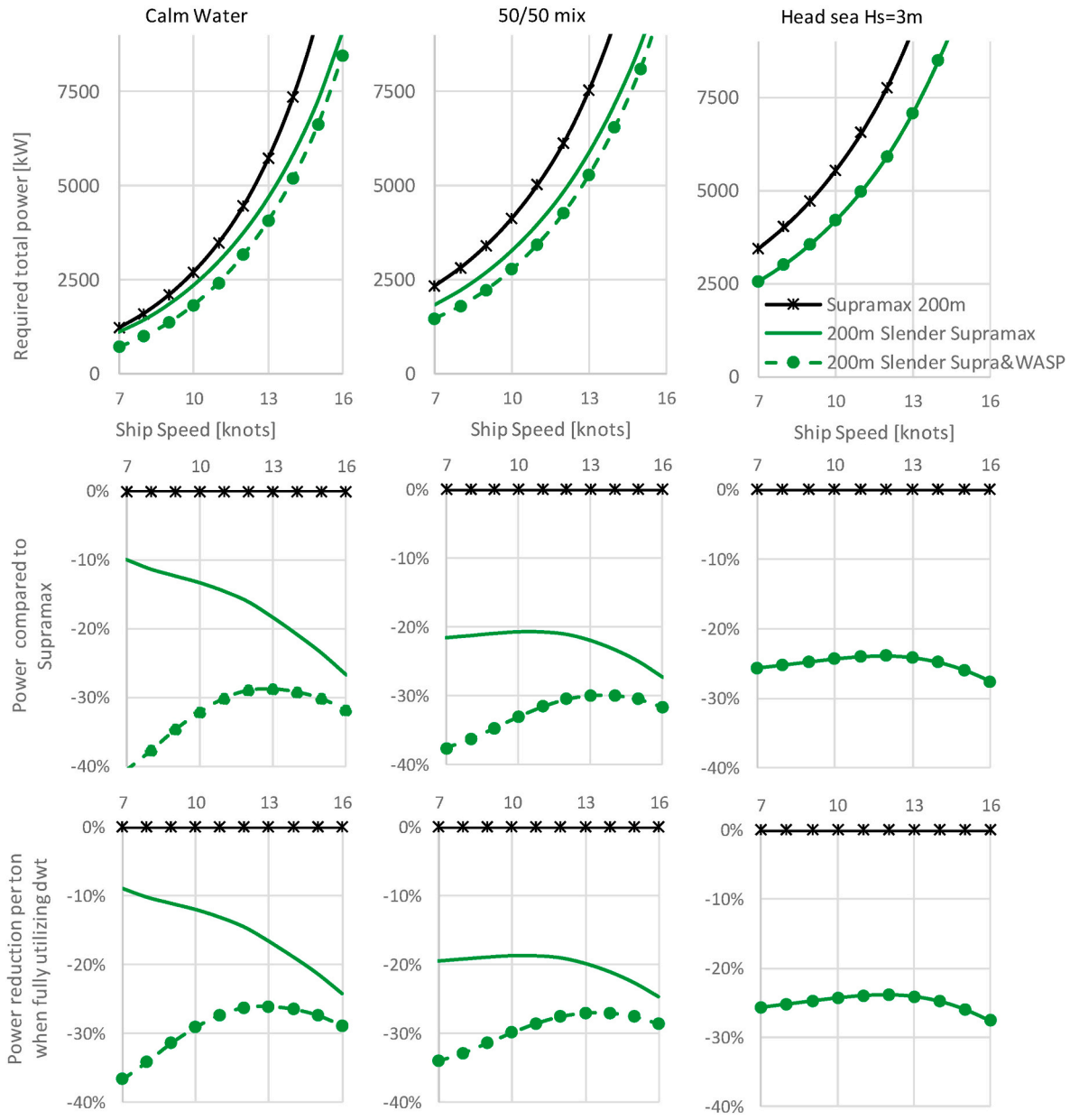

Fig. 4. Required power as a function of speed and sea conditions when loaded.

calm water conditions when averaged out over all wave heights, side waves give added resistance and head waves gives the full added resistance. Interaction between vessel and waves is simplified into an annual pattern of a 50%–50% distribution between calm sea conditions and 3m head waves to reflect average annual global in line with Lindstad et al. (2011) and Lindstad et al. (2019). With this approach we ensure that the added resistance from real sea is included in the total power required and that we hence also avoid overestimating the percentage of power reduction with WASP installed. The 3m significant wave height is also in line with the average significant wave height obtained from the Pierson-Moskowitz spectrum (see Fig. 1). Moreover, as already stated, we assume that the propulsion power from the WASP units (which in any case are zero for the percentage of the time the vessel operates in head wind conditions) aligns with the coefficient 0.5 smarts in Fig. 2 because of tiltable rotors and moderate voyage adjustments.

The main observations from Fig. 4 are: First the solid green line shows performance of the 200m Slender Supramax without WASP compared to the 200m Supramax, while the dotted and dashed green line shows what we in total achieve when we also add WASP; Second, at calm water the Slender Supramax use 10% less power, and the advantage gradually increases to more than 20% less at speeds above 14 knots; Third, in headwind conditions, slenderness on its own gives around 25% power reductions (With wind contributing zero in headwinds, the lines with and without WASP are plotted on top of each other); Fourth, the 50/50 distribution between calm sea and 3m head waves appears to be a good benchmark to compare vessels with and without WASP and the results indicates that the 200m Slender Supramax with WASP requires nearly 35% less power at low speeds, around 30% at 10 knots and 27% less at 13 knots in loaded conditions. Fifth, for pure headwind conditions, the WASP will not contribute with any propulsion power, so the plotted dot is just used to indicate the relative magnitude of the wind.

In the following parts of this analysis, we use the 50/50 mix for sea conditions, and we assume that very few cargo shipments will exceed the dwt capacity of the 200m Slender Supramax based on its capacity on 13.4m draught, which anyhow has a similar dwt capacity in ports where it can utilize its larger maximum draught of 14.4m (compared to the

13.4m for the typical Supramax). Fig. 5 shows the required power as a function of vessel speed with the reference 50/50 sea conditions for three different loading conditions: Ballast, a 50/50 mix between ballast and loaded, and fully loaded. Three alternative options are compared: Supramax 200m, 200m Slender Supramax and the 200m Slender Supramax with WASP.

The main observation from Fig. 5 is that we get the largest power, and hence fuel and emissions reduction compared to the typical Supramax, when the alternative designs are fully loaded, and the smallest reduction when sailing in ballast. Moreover, the results indicate that using a 50/50 mix of ballast and loaded gives a good average of the advantage of WASP solutions both with Sail Routing and without. It could be argued that 60/40 or even a 70/30 split between loaded voyages and ballast would have been more representative of Supramax vessels trading pattern. However, by using 50/50 we are not overestimating the benefits of the 200m Slender Supramax with WASP. In the next sections, we use the 50/50 for ballast and loaded and the 50/50 split for calm and significant wave height $H_s = 3$m.

Fig. 6 shows Daily cost and required power as a function of speed in the top row, and Power and Cost per nm as a function of speed in the bottom row. From Fig. 6, we see that both power and cost increase in absolute values when the speed increases, as shown in the top row. Moving from absolute values to power and cost per nm in the bottom row, we observe that, with a fuel cost of 500 USD/TOE, the Supramax 200m achieves the lowest cost per nm at a speed of 13 knots, and if fuel cost is doubled, i.e., 1000 USD/TOE, that reduces cost minimizing speed with 1–2 knots. Second, with a fuel cost of 500 USD/TOE, the 200m Slender Supramax with WASP achieves the lowest cost with speeds in the range of 12–14 knots, and if fuel cost is doubled it achieves the lowest cost at a speed around 10 knots. Third, the 200m Slender Supramax with WASP has a cost advantage even with the lowest fuel cost, and if fuel cost is doubled, the cost advantage increases from around 10% with a speed of 12 knots to around 15% with a speed of 10 knots. If we use 11 knots and the lowest fuel price, the annual cost of the Supramax 200m (Capex + Opex + fuel) comes at 5.8 MUSD with an annual fuel consumption of 4134 TOE, when sailing at sea. In comparison, the 200m Slender Supramax with WASP comes at 5.6 MUSD with an annual fuel consumption of 3025 TOE, i.e., a 27% saving on fuel and GHG emissions.

We now compare the cost of a 100% decarbonising through zero carbon fuels only, with the cost if zero fuels are combined with slender designs and wind assisted propulsion. This is done by replacing E-ammonia with the VLSFO and obtain the results displayed in Fig. 7. As E-fuel price estimates, we use 1750 USD per TOE of E-ammonia (Lindstad et al., 2021), and 2975 USD per TOE to reflect the much higher energy prices seen in March 2022 compared to prices in the spring and summer of 2021. 1750 USD per TOE corresponds to an electricity price of 60 USD per MWh, and 2975 USD, to an electricity price of 120 USD per MWh.

The main observations from Fig. 7 are: First, that the daily cost difference between the 200m Slender Supramax with WASP increases as a function of E-ammonia being more expensive than VLSFO, as shown in the upper right corner; Second, moving from absolute values to power and cost per nm in the bottom row, we observe that with an E-ammonia cost of 1750 USD/TOE the Supramax 200m achieves the lowest cost

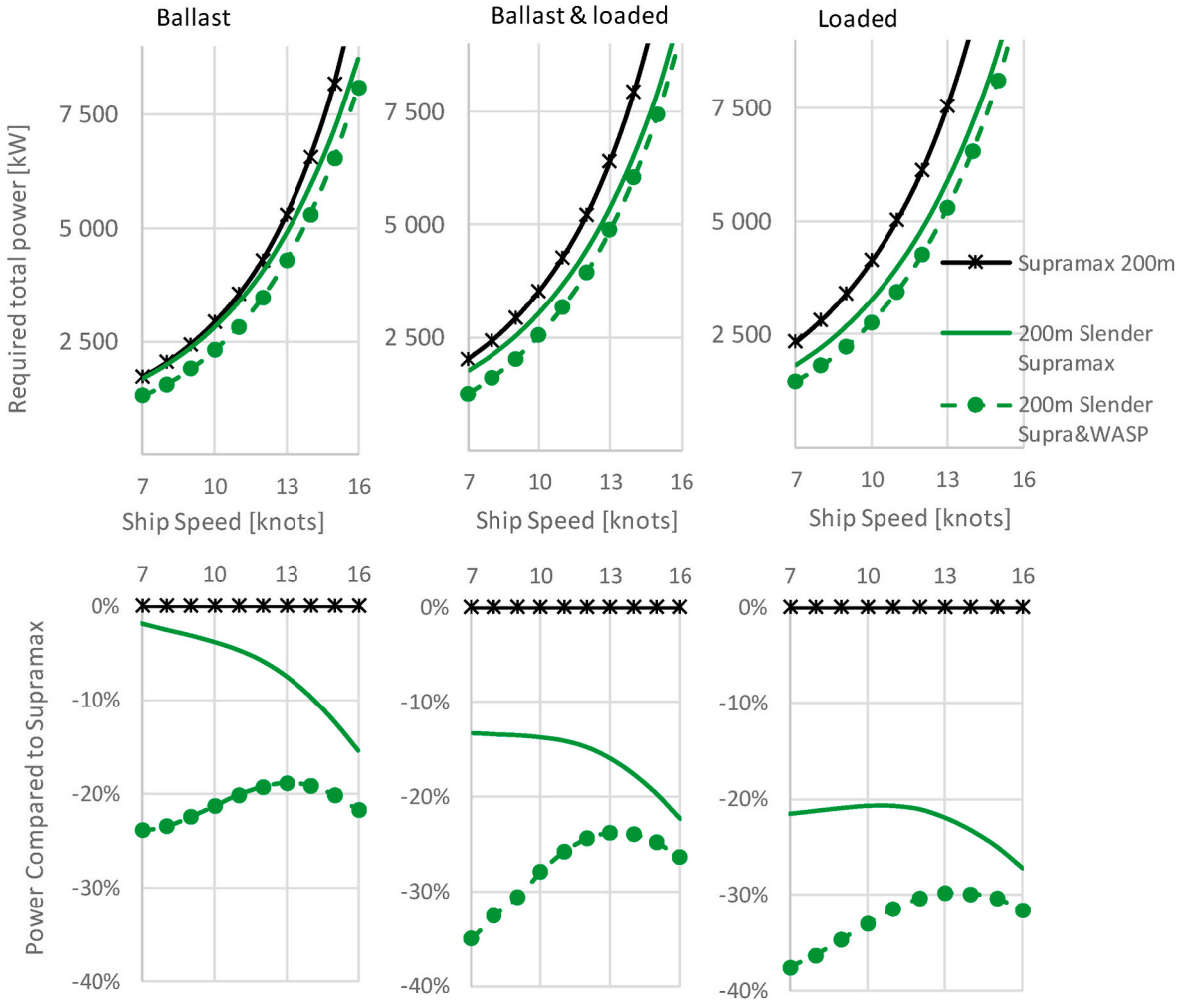

Fig. 5. Required power as a function of loading condition and speed.

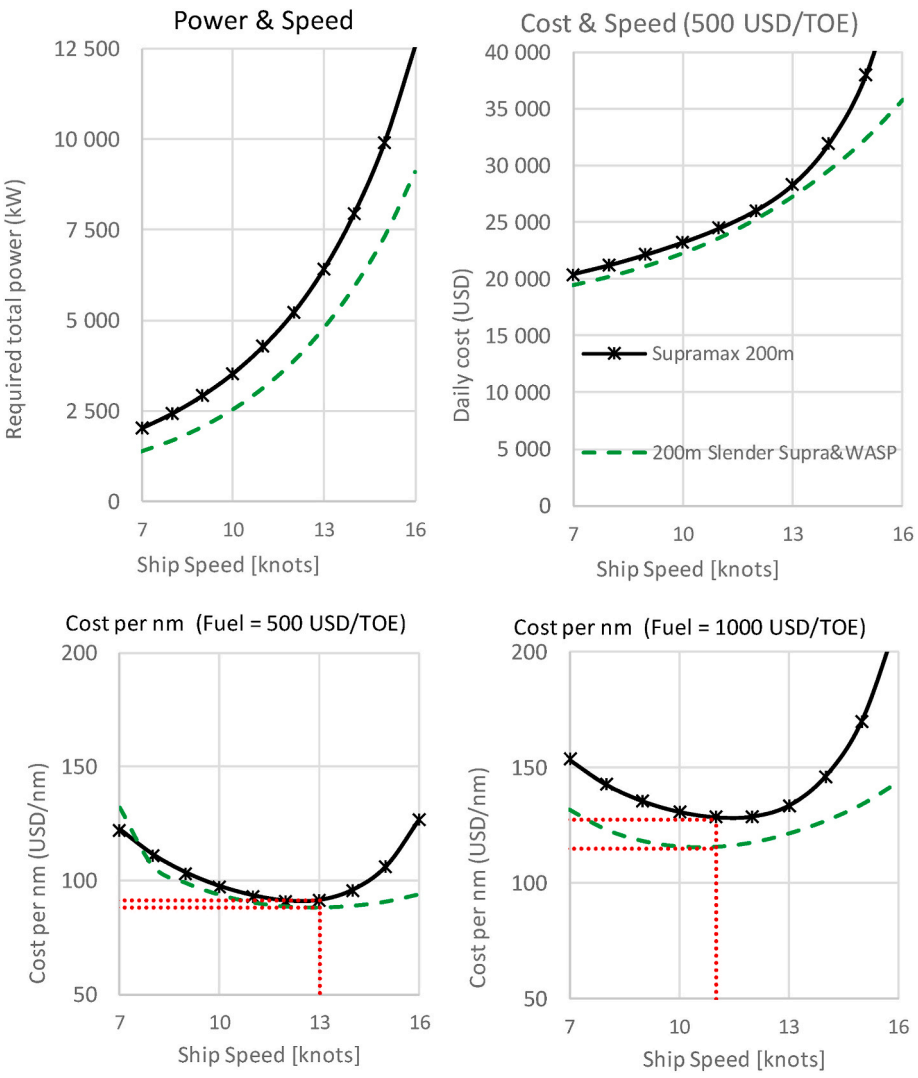

Fig. 6. Daily cost and required power in absolute values and per nautical mile.

with a speed of around 11 knots, while the 200m Slender Supramax achieves the lowest cost with speeds around 10 knots. Third, with E-ammonia, the cost advantage of the 200m Slender Supramax increases compared to when the conventional fuel is used. At 11 knots and an E-ammonia price of 1750 USD/TOE, the annual cost of the Supramax 200m (Capex + Opex + fuel) comes at 12.5 MUSD with an annual fuel consumption of 4134 TOE, when sailing at sea. In comparison, the 200m Slender Supramax with WASP comes at 10 MUSD with an annual fuel consumption of 3025 TOE, i.e., a 27% lower energy consumption. Finally, with an E-ammonia price of 2975 USD/TOE the cost becomes so high that it makes no sense to make any comments at all.

Table 3 summarizes the main results of this study.

The main results found are: First, building more slender bulk vessels in combination with wind assisted propulsion reduces fuel consumption and GHG emissions by 27% at an abatement cost of −50 USD per ton of CO_2; Second, when combining slender hull and wind with Zero carbon fuels, a 100% GHG reduction comes at an abatement cost of 328 USD per ton of CO_2, which still is significantly less than the 459 USD per ton of CO_2 using Zero carbon fuels only.

5. Conclusions

This study has focused on decarbonizing bulk shipping by combining ship design and alternative power. The results indicate: First, that fuel consumption and emissions can be reduced by around 25% through more slender designs enabled by increased maximum draughts and wind assisted propulsion and that the two measures are fully paid back through the reduced fuel bill. These fuel and emission reductions are of a similar magnitude as what Lindstad et al. (2022) reported when the slenderness was achieved through increasing the length from 200 to 229m. However, while the extended length option increased building cost significantly and needed a fuel price at the present peak level or above (100 USD per barrel) to be profitable, the extended draught option as investigated here does not increase building cost and hence gives large emission reductions free of charge.

Second, combining a more slender hull and WASP with Zero carbon fuels to achieve a 100% GHG reduction comes at a significantly lower annual abatement cost of 4.607 MUSD compared to 6.444 MUSD with Zero carbon fuels only; Third, there is a need for further research and projects to fully investigate the potential of combining more slender hull forms with WASP to confirm the potential and provide to shipowners robust information basis for investment in such ships.

CRediT authorship contribution statement

Elizabeth Lindstad: Conceptualization, Data curation, Methodology, Formal analysis, Investigation, Validation, Writing – original draft. **Dražen Polić:** Methodology, Formal analysis, Validation, Software,

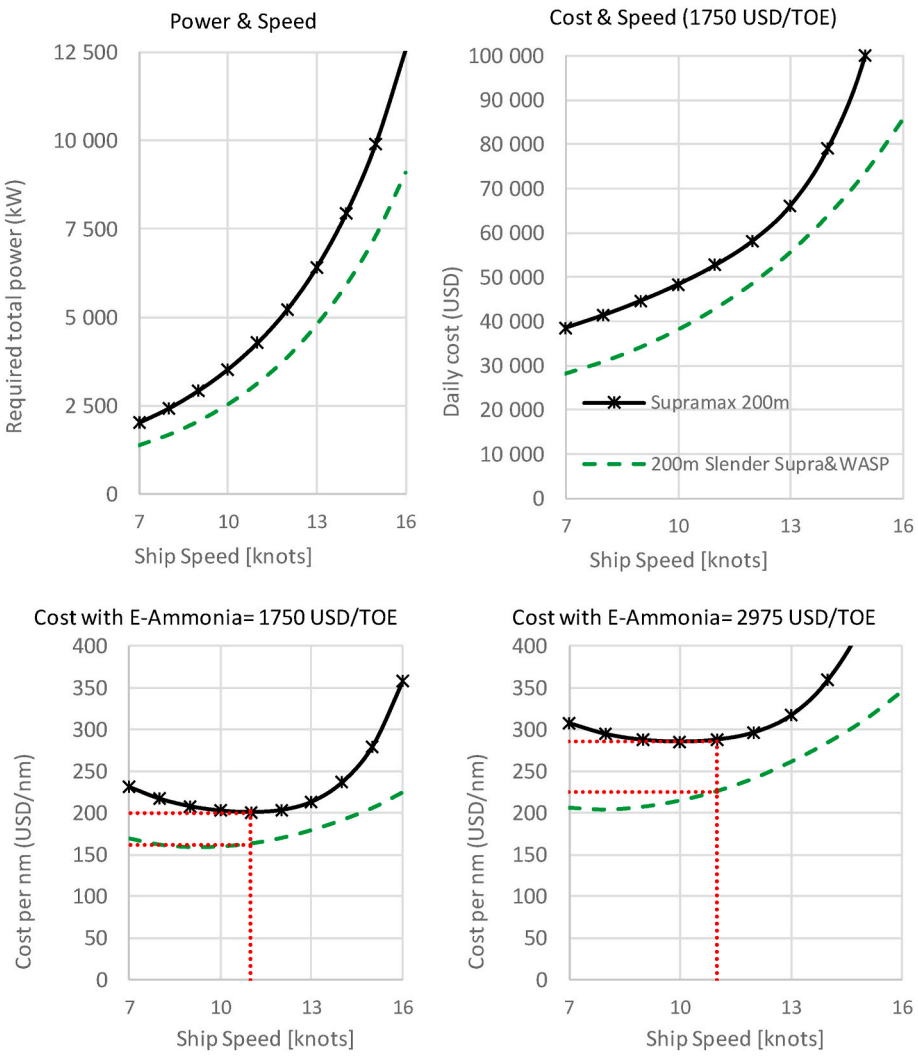

Fig. 7. Daily cost and required power in absolute values and per nautical mile.

Table 3
Abatement cost and CO2 reductions.

Fuel	Supramax 200m	200m Slender Supramax with WASP	200m Slender Supramax with WASP	Supramax 200m
	VLSFO	VLSFO	E-Ammonia	E-Ammonia
Annual Cost (USD)	5 944 000	5 756 000	10 551 000	12 388 000
Annual CO_2 emissions (ton)	14 032			
CO_2 reduction (ton)		3 765	14 032	14 032
CO_2 reduction (%)		27%	100%	100%
Abatement cost (USD)		−188 000	4 607 000	6 444 000
Abatement cost per ton (USD/ton of CO_2)		-50	328	459

Visualization, Writing – original draft. **Agathe Rialland:** Methodology, Project administration, Visualization, Writing – review & editing. **Inge Sandaas:** Investigation, Validation, Writing – review & editing. **Tor Stokke:** Investigation, Validation, Writing – review & editing.

Declaration of competing interest

The authors declare that they have no known competing financial interests or personal relationships that could have appeared to influence the work reported in this paper.

Data availability

Data will be made available on request.

Acknowledgement

The authors would like to thank the reviewers for all constructive and insightful comments, which contributed to significant improvements to the manuscript. This study has been financially supported by the Norwegian Research Council's (Norges Forskningsråd) projects 237917 - SFI Smart Maritime, and 294771 - CLIMMS. SFI Smart Maritime is the Norwegian centre for improved energy efficiency and reduced harmful emissions from maritime transport. CLIMMS focuses on Climate change mitigation in the maritime sector and Developing pathways for the transformation of the international shipping sector towards the IMO goal for 2050.

References

Alvarez, J.F., Engebretsen, E., Longva, T., 2010. The Environmental Impact of Port Queuing Policies. IAME July 2010, Lisbon Portugal.

Balcombe, P., Brierley, J., Lewis, C., Skatvedt, L., Speirs, J., Hawkes, A., Staffell, I., 2019. How to decarbonise international shipping: options for fuels, technologies and policies. Energy Convers. Manag. 182, 72–88.

Bausch, D.O., Brown, G.G., Ronen, D., 1998. Scheduling short term marine transport of bulk products. Marit. Pol. Manag. 25 (4), 335–348.

Bengtsson, N., 2018. Shipping market update. In: Proceedings of the International Maritime Statistics Forum, Hamburg, Germany, 17–19 April 2018.

Bordogna, G., Muggiasca, S., Giappino, S., Belloli, M., Keuning, J., Huijsmans, R., van 't Veer, A., 2019. Experiments on a Flettner rotor at critical and supercritical Reynolds numbers. J. Wind Eng. Ind. Aerod. 188, 19–29.

Bouman, E.A., Lindstad, E., Rialland, A.I., Strømman, A.H., 2017. State-of-the-Art technologies, measures, and potential for reducing GHG emissions from shipping - a Review. Transport. Res. Part D 52, 408–421, 2017.

Cho, S.C., Perakis, A.A., 1996. Optimal liner fleet routing strategies. Marit. Pol. Manag. 23 (1996), 249–259.

Chou, T., Kosmas, V., Acciaro, M., Renken, K., 2021. Comeback of wind power in shipping: an economic and operational review on the wind-assisted ship propulsion technology. Sustainability 13, 1880–1896.

Christiansen, M., Fagerholt, K., Ronen, D., Nygren, B., 2007. Maritime transportation. In: Barnhart, C., Laporte, G. (Eds.), Handbook in Operations Research and Management Science. Elsevier, 2007.

Corbett, J.J., Wang, H., Winebrake, J.J., 2009. The effectiveness and cost of speed reductions on emissions from international shipping. Transport. Res. D 14, 593–598, 2009.

Council of the European Union, 2015. Regulation (EU) 2015/757 of the European Parliament and of the Council of 29 April 2015 on the monitoring, reporting and verification of carbon dioxide emissions from maritime transport, and amending directive 2009/16/EC. Off. J. Eur. Union 58, 55–76.

Fagerholt, K., 2001. Ship scheduling with soft time windows - an optimization based approach. Eur. J. Oper. Res. 131, 559–571, 2001.

Fagerholt, K., Lindstad, E., 2000. Optimal policies for maintaining a supply service in the Norwegian Sea. Omega 28, 269–275, 2000.

Fagerholt, K., Johnsen, A.V., Lindstad, E., 2009. Fleet deployment in liner shipping - a case study. Marit. Pol. Manag. 2009 (5), 397–409.

Fairplay, 2018. Pace race - slow steaming not a Sulphur cap saviour. Fairplay 391, 24–26, 13 September 2018.

Faltinsen, O.M., Minsaas, K.J., Liapis, N., Skjørdal, S.O., 1980. Prediction of Resistance and Propulsion of a Ship in a Seaway. 13th Symposium on Naval Hydrodynamics. the Shipbuilding Research Association of Japan, Tokyo.

Garzon, F., Figueroa, A., 2017. The study on the flow generated by an array of four flettner rotors: theory and experiment. Appl. Math. 1851–1858, 08.

Hirota, K., Matsumoto, K., Takagishi, K., Yamasaki, K., Orihara, H., Yoshida, H., 2005. Development of bow shape to reduce the added resistance due to waves and verification on full scale measurement. In: International Conference on Marine Research and Transportation, 2005, Italy.

HOLTROP, J.A., 1984. Statistical reanalysis of resistance and propulsion data. Int. Shipbuild. Prog. 31, 272–276.

IEC, 2019. IEC 61400-3-1. Wind Energy Generation Systems - Part 3-1: Design Requirements for Fixed Offshore Wind Turbines, 2019.

IPCC, 2021. AR6 Climate Change-The Physical Science Basis. https://www.ipcc.ch/report/ar6/wg1/.

ITTC, 2014. Preparation and Conduct of Speed Power Trials 27th International Towing Tank Conference.

Kramer, J.V., Steen, S., 2022. Simplified test program for hydrodynamic CFD simulations of wind-powered cargo ships. Ocean Eng. 244, 110297.

Kramer, J.A., Steen, S., Savio, L., 2016. Drift forces-wing-sails vs Flettner rotors. Cortona. In: Proceedings High Performance Marine Vehicles.

Kristensen, H.O.H., 2010. Model for Environmental Assessment of Container Ship Transport. The Society of Naval Architects and Marine Engineers (SNAME), Seattle, USA, 3.- 5. November.

Kumar, S., Hoffman, J., 2002. Globalisation the maritime nexus. In: Grammenos, C.T. (Ed.), The Handbook of Maritime Economics and Business. LLP, ISBN 1-84311-195-0, pp. 35–64.

Lagemann, B., Lindstad, E., Fagerholt, K., Rialland, A., Erikstad, S., 2022. Optimal ship lifetime fuel and power system selection. Transport. Res. Part D 2022 (102), 103145.

Lewis, E.D., 1988. Principles of Naval Architecture, vol. II. The Society of Naval Architects and Marine Engineers. ISBN0-939773-01-5.

Lindstad, E., Asbjørnslett, B.E., Strømman, A.H., 2011. Reductions in greenhouse gas emissions and cost by shipping at lower speed. Energy Pol. 39, 3456–3464.

Lindstad, E., Jullumstrø, E., Sandaas, I., 2013. Reduction in cost and emissions with new bulk ships designs enabled by the Panama Canal expansion. Energy Pol. 59, 341–349, 2013.

Lindstad, E., Borgen, H., Eskeland, G.S., Paalson, C., Psaraftis, H., Turan, O., 2019. The need to amend IMO's EEDI to include a threshold for performance in waves (realistic sea conditions) to achieve the desired GHG reductions. Sustainability 11, 3668, 2019. https://doi:10.3390/su11133668.

Lindstad, E., Eskeland, G.S., Rialland, A., Valland, A., 2020. Decarbonizing maritime transport: the importance of engine technology and regulations for LNG to serve as a transition fuel. Sustainability 12 (5), 8793, 2020.

Lindstad, E., Lagemann, B., Rialland, A., Gamlem, G.M., Valland, A., 2021. Reduction of maritime GHG emissions and the potential role of E-fuels. Transport. Res. Part D 101 (2021), 103075.

Lindstad, E., Stokke, T., Alterskjær, A., Borgen, H., Sandaas, I., 2022. Ship of the future - a slender dry-bulker with wind assisted Propulsion. Maritime Transport Research 3, 100055, 2022.

Lloyd, A.R.J.M., 1998. Seakeeping, Ship Behaviour in Rough Weather, ISBN 0-9532634-0-1.

Lloyd's List Intelligence, 2019. Shipbuilding Outlook. Informa UK Limited, London, UK. May 2019, issue 83.

LR, 2021. https://flettner.lr.org/.

Lu, R., Ringsberg, J.W., 2020. Ship energy performance study of three wind-assisted ship propulsion technologies including a parametric study of the Flettner rotor technology. Ships Offshore Struct. 15 (3), 249–258.

Norstad, I., Fagerholt, K., Laporte, G., 2010. Tramp shipping routing and scheduling with optimization. Transport. Res. Part C 19 (5), 853–865.

Pavia, E.G., O'Brien, J.J., 1986. Weibull statistics of wind speed over the ocean. J. Appl. Meteorol. Climatol. 25 (10), 1324–1332.

Psaraftis, H.N., Kontovas, C.A., 2010. Balancing the economic and environmental performance of maritime transport. Transport. Res. Part D 15, 458–462, 2010.

Rehmatulla, N., Parker, S., Smith, T., Stulgis, V., 2017. Wind technologies: opportunities and barriers to a low carbon shipping industry. Marine Policy, Issue 75, 217–226.

Rojon, I., Dieperink, C., 2014. Blowin'in the wind? Drivers and barriers for the uptake of wind propulsion in international shipping. Energy Policy, Issue 67, 394–402.

SHELL, 2021. The Energy Transformation Scenarios. https://www.shell.com.

Silverleaf, A., Dawson, J., 1966. Hydrodynamic Design of Merchant Ships for Highspeed Operation. Summer Meeting in Germany 12th - 16th of June, 1966. The Schiffbau-Technische Gescaft E.V, the Institute of Engineers and Shipbuilders in Scotland, the North East Coast Institution of Engineers and Shipbuilders. The Royal institution of naval architects.

Smith, T.W.P., Jalkanen, J.-P., Anderson, B.A., Corbett, J.J., Faber, J., Hanayama, S., O'Keeffe, E., Parker, S., Johansson, L., Aldous, L., Raucci, C., Traut, M., Ettinger, S., Nelissen, D., Lee, S., Ng, D.S., Agrawal, A., Winebrake, J.J., Hoen, M., Chesworth, S., Pandey, A., 2015. Third IMO GHG Study 2015. International Maritime Organization (IMO), London, UK.

SSI, 2019. The Role of Sustainable Biofuels in the Decarbonization of Shipping: the findings of an inquiry into the sustainability and availability of biofuels for shipping. https://www.sustainableshipping.org/news.

Stott, P., Wright, P., 2011. Opportunities for improved efficiency and reduced CO2 emissions in dry bulk shipping stemming from the relaxation of the Panamax beam constraint. Int. J. Marit.Eng 153 (A4), A215–A229.

Svanberg, M., Ellis, J., Lundgren, J., Landälv, I., 2018. Renewable methanol as a fuel for the shipping industry. Renew. Sustain. Energy Rev. 94, 1217–1228.

Tillig, F., Ringsberg, J.W., 2020. Design, operation and analysis of wind-assisted cargo ships. Ocean Eng. 211, 107603.

UNCTAD, 2021. Review of Maritime Transport. www.unctad.org.

van den Boom, H.J.J., Hasselaar, T.W.F., 2014. Ship speed-power performance assessment. Transactions 122, 2014. https://doi.org/10.5957/SMC-2014-T04. SNAME Maritime Convention 2014, October 2014 Houston, Texas.

van der Tempel, J., 2006. Design of Support Structures for Offshore Wind Turbines. PhD thesis. Delft University of Technology.